

RESEARCH ARTICLE | AUGUST 22 2024

Improved memory truncation scheme for quasi-adiabatic propagator path integral via influence functional renormalization

Limin Liu  ; Jiajun Ren   ; Weihai Fang 

 Check for updates

J. Chem. Phys. 161, 084101 (2024)

<https://doi.org/10.1063/5.0221916>


View
Online


Export
Citation

Articles You May Be Interested In

Coarse-grained representation of the quasi adiabatic propagator path integral for the treatment of non-Markovian long-time bath memory

J. Chem. Phys. (June 2017)

PATHSUM: A C++ and Fortran suite of fully quantum mechanical real-time path integral methods for (multi-)system + bath dynamics

J. Chem. Phys. (June 2023)

Path-integral methodology and simulations of quantum thermal transport: Full counting statistics approach

J. Chem. Phys. (February 2019)



The Journal of Chemical Physics
**Special Topics Open
for Submissions**

Learn More

 AIP
Publishing

Improved memory truncation scheme for quasi-adiabatic propagator path integral via influence functional renormalization

Cite as: J. Chem. Phys. 161, 084101 (2024); doi: 10.1063/5.0221916

Submitted: 4 June 2024 • Accepted: 5 August 2024 •

Published Online: 22 August 2024



View Online



Export Citation



CrossMark

Limin Liu, Jiajun Ren,^{a)} and Weihai Fang

AFFILIATIONS

Key Laboratory of Theoretical and Computational Photochemistry, Ministry of Education, College of Chemistry, Beijing Normal University, 100875 Beijing, People's Republic of China

^{a)}Author to whom correspondence should be addressed: jjren@bnu.edu.cn

ABSTRACT

Accurately simulating non-Markovian quantum dynamics in system–bath coupled problems remains challenging. In this work, we present a novel memory truncation scheme for the iterative quasi-adiabatic propagator path integral (iQuAPI) method to improve accuracy. Conventional memory truncation in iQuAPI discards all influence functional beyond a certain time interval, which is not effective for problems with a long memory time. Our proposed scheme selectively retains the most significant parts of the influence functional using the density matrix renormalization group algorithm. We validate the effectiveness of our scheme through simulations of the spin–boson model across various parameter sets, demonstrating faster convergence and improved accuracy compared to the conventional scheme. Our findings suggest that the new memory truncation scheme significantly advances the capabilities of iQuAPI for problems with a long memory time.

Published under an exclusive license by AIP Publishing. <https://doi.org/10.1063/5.0221916>

I. INTRODUCTION

System–bath coupled models provide a microscopic description of dissipative quantum processes in the condensed phase,¹ such as spectroscopy and energy transfer in protein environments in light-harvesting complexes,^{2,3} optoelectronic processes in organic semiconductors,^{4,5} and quantum transport in molecular electronic devices.^{6,7} The theoretical investigation of the dynamics of system–bath models is essential for understanding the macroscopic phenomena observed in experiments from a microscopic perspective.

However, it remains a significant challenge to simulate the quantum dynamics of system–bath models with high accuracy beyond the common perturbative and Markovian approaches. The wavefunction approaches, including the multilayer multiconfiguration time-dependent Hartree (ML-MCTDH)^{8,9} and time-dependent density matrix renormalization group (TD-DMRG) approaches,^{10,11} treat the system and bath degrees of freedom (DOFs) on an equal footing. For condensed phase problems, hundreds or thousands of discrete bath modes need to be treated explicitly for a single bath, making it difficult to extend to more complex problems with

multiple baths. When only the dynamics of the system part is of interest, it is more common to calculate the reduced dynamics of the system by treating the bath DOFs implicitly and *a priori*. Nevertheless, the memory effect induced by the bath makes the reduced dynamics of the system non-Markovian—the dynamics depends on all the historical information of the system part, which is also called temporal correlation.^{12,13}

There are many numerically exact reduced quantum dynamics approaches that have been proposed, including hierarchical equations of motion (HEOM),^{7,14–16} quasi-adiabatic propagator path integral (QuAPI),^{17–19} stochastic Schrödinger equation (SSE),^{4,20,21} and generalized quantum master equation (GQME).^{22,23} Among them, QuAPI, developed by Makri and co-workers, based on the Feynman and Vernon influence functional theory,²⁴ can, in principle, handle arbitrary bath spectral density and zero temperature, making it very compelling. The practically used iterative QuAPI (iQuAPI) approach and its variants are not only widely adopted to benchmark other methods but also applied to many real-world problems.^{25–27} However, the computation and storage of the central quantity in QuAPI, the augmented reduced density tensor (ARDT), increases exponentially with respect to the physical memory time.

To make numerical simulation feasible, the memory time must be truncated in practice, known as the finite memory approximation. The truncation length can be regarded as a parameter that needs to be converged. For problems with long memory, it has been found that convergence is very challenging with this conventional truncation scheme in iQuAPI.²⁸

Many algorithms have been proposed to improve the accuracy of QuAPI when dealing with problems with long memory, including the path filtering,²⁹ the blip decomposition,³⁰ the coarse graining,³¹ the scaling coefficient of influence functional,²⁸ and the kink sum.³² The more recently developed time-evolving matrix product operator approach (TEMPO) and its variants use matrix product operators to represent the influence functional and matrix product states (MPS) to approximate ARDT, which can greatly improve the efficiency of QuAPI for problems with long memory.^{33–40} The small matrix decomposition of the path integral approach (SMatPI) and its extended memory algorithm (x-SMatPI), developed by Makri, disentangles the original path integral recursively, and thus, the residual terms are negligible and can be discarded. As a result, the storage of the original exponentially large ARDT can be replaced with small matrices with only two time indices.^{41–43}

In this work, based on the iQuAPI approach, we propose a new memory truncation scheme that improves the accuracy of the conventional scheme. The idea of the scheme is that the influence functional beyond a certain time interval is not fully discarded as in the original iQuAPI algorithm, but the most important part is selected and retained according to the density matrix renormalization group theory (DMRG).^{44,45} In our method, an auxiliary time slice is introduced, which is the renormalization of all the historical time slices beyond a certain time interval. The effectiveness of our method is demonstrated by comparing it with the conventional iQuAPI method for simulating quantum dynamics of the spin-boson model with a relatively long memory time.

The remaining sections of this paper are arranged as follows: in Sec. II, we briefly recap the iQuAPI algorithm and present the detailed algorithm of our memory truncation scheme. In Sec. III, we show the numerical results of the quantum dynamics of the spin-boson model. Finally, we present our conclusions in Sec. IV.

II. METHODS

A. System-bath model and iQuAPI approach

System-bath models are widely used to study quantum dissipative dynamics in the condensed phase. In this work, we only consider bosonic baths. The generic Hamiltonian is written as

$$\hat{H} = \hat{H}_S + \hat{H}_B + \hat{H}_{SB}, \quad (1)$$

$$\hat{H}_B = \sum_i \frac{1}{2} \hat{p}_i^2 + \frac{1}{2} \omega_i^2 \hat{q}_i^2, \quad (2)$$

$$\hat{H}_{SB} = \sum_n \hat{S}_n \otimes \sum_i c_{ni} \hat{q}_i. \quad (3)$$

Here, \hat{H}_S is the system Hamiltonian, which is assumed to be simple to solve. \hat{H}_B is the bath Hamiltonian, composed of independent harmonic modes with frequency ω_i for mode i . \hat{H}_{SB} is the interaction

between the system and bath, in which the system operator \hat{S}_n is linearly coupled to the coordinates of the bath with coupling strength c_{ni} .

The reduced density matrix of the system part after tracing the whole density matrix over the bath part is $\rho_S(t) = \text{Tr}_B \rho(t)$. With reduced quantum dynamics approaches, an effective equation of motion of $\rho_S(t)$ under the influence of the bath is to be solved.

The QuAPI method was proposed to solve the reduced quantum dynamics and has been described in detail in a previously excellent review.⁴⁶ For simplicity, we only consider one coupling term in Eq. (3), and thus, the summation over n is neglected. The extension to multiple coupling terms with both diagonal and off-diagonal system-bath couplings is referred to in Refs. 47–49. In QuAPI, the Hamiltonian is re-partitioned into

$$\hat{H} = \hat{H}_0 + \hat{H}_1, \quad (4)$$

$$\hat{H}_0 = \sum_i \frac{1}{2} \hat{p}_i^2 + \frac{1}{2} \omega_i^2 \left(\hat{q}_i + \frac{c_i \hat{S}}{\omega_i^2} \right)^2, \quad (5)$$

$$\hat{H}_1 = \hat{H}_S - \sum_i \frac{c_i^2 \hat{S}^2}{2\omega_i^2}. \quad (6)$$

With this partition, the formal propagator is split approximately by Trotter decomposition. For clarity, the equations in this section are presented with first-order Trotter splitting $e^{-i\hat{H}\Delta t} \approx e^{-i\hat{H}_0\Delta t} e^{-i\hat{H}_1\Delta t}$. However, in our calculations in Sec. III, the second-order Trotter splitting ($e^{-i\hat{H}\Delta t} \approx e^{-i\hat{H}_1\Delta t/2} e^{-i\hat{H}_0\Delta t} e^{-i\hat{H}_1\Delta t/2}$) is used for higher accuracy. The extension of the first-order formulation to second-order formulation is straightforward, similar as Refs. 18 and 19. After inserting multiple resolutions of identity and integrating out the bath part analytically, the evolution of the reduced density matrix of the system is expressed as the path integral with N time slices,

$$\begin{aligned} \rho_S(N\Delta t) &= \text{Tr}_B \langle s_N^+ | e^{-i\hat{H}N\Delta t} \rho(0) e^{i\hat{H}N\Delta t} | s_N^- \rangle \\ &= \int ds_0^+ \cdots \int ds_{N-1}^+ \int ds_0^- \cdots \int ds_{N-1}^- \\ &\times \langle s_0^+ | \rho_S(0) | s_0^- \rangle B(s_0^\pm, s_1^\pm, \dots, s_N^\pm) F(s_1^\pm, s_2^\pm, \dots, s_N^\pm), \end{aligned} \quad (7)$$

where $\rho(0)$ is assumed to be factorized $\rho(0) = \rho_S(0)\rho_B^{\text{eq}}$. The formulation to simulate the equilibrium initial state is given in Refs. 50 and 51. Here, $|s\rangle$ is the eigenstate of the system operator \hat{S} with eigenvalue s . The superscript \pm indicates the forward and backward propagation, respectively. For clarity, in the following, the variable in parentheses of each tensor is omitted if possible. B is the bare system propagator, written as

$$B(s_0^\pm, s_1^\pm, \dots, s_N^\pm) = \prod_{k=1}^N K_{k-1,k}, \quad (8)$$

$$K_{k-1,k} := K_{k-1,k}(s_{k-1}^\pm, s_k^\pm), \quad (9)$$

$$= \langle s_k^+ | e^{-i\hat{H}_1\Delta t} | s_{k-1}^+ \rangle \langle s_{k-1}^- | e^{i\hat{H}_1\Delta t} | s_k^- \rangle. \quad (10)$$

F is the discrete Feynman–Vernon influence functional, which can be decomposed into the products of pairwise components $I_{k'k}$ ($k' \leq k$). The influence functional describes the influence of the bath on system dynamics and introduces temporal correlation,

$$F(s_1^\pm, s_2^\pm, \dots, s_N^\pm) = \prod_{k=1}^N \prod_{k'=1}^k I_{k'k}, \quad (11)$$

$$I_{k'k} := I_{k'k}(s_k^\pm, s_k^\pm) = \exp [-(s_k^+ - s_k^-)(\eta_{k'k}s_{k'}^+ - \eta_{k'k}^*s_{k'}^-)]. \quad (12)$$

The coefficient $\eta_{k'k}$ only depends on $\Delta k = k - k'$, which is expressed as¹⁸

$$\begin{aligned} \eta_{k'k} &= \frac{2}{\pi} \int_{-\infty}^{\infty} d\omega \frac{J(\omega)}{\omega^2} \frac{\exp(\beta\omega/2)}{\sinh(\beta\omega/2)} \sin^2(\omega\Delta t/2) e^{-i\omega\Delta t(k-k')}, \quad k' < k, \\ \eta_{kk} &= \frac{1}{2\pi} \int_{-\infty}^{\infty} d\omega \frac{J(\omega)}{\omega^2} \frac{\exp(\beta\omega/2)}{\sinh(\beta\omega/2)} (1 - e^{-i\omega\Delta t}), \quad k' = k, \end{aligned} \quad (13)$$

in which $J(\omega)$ is the bath spectral density, $J(\omega) = \frac{\pi}{2} \sum_i \frac{c_i^2}{\omega_i} \delta(\omega - \omega_i)$.

To propagate Eq. (7) in an iterative way, the influence functional F in Eq. (11) can be grouped as

$$F = \prod_{k=1}^N f_k, \quad (14)$$

$$f_k := f_k(s_1^\pm, s_2^\pm, \dots, s_k^\pm) = \prod_{k'=1}^k I_{k'k}, \quad (15)$$

where f_k contains all the pairwise subterms of the influence functional between k and k' ($k' \leq k$). With this decomposition of F , the key quantity in QuAPI called augmented reduced density tensor A_k can be iteratively calculated as

$$A_k := A_k(s_1^\pm, \dots, s_k^\pm), \quad (16)$$

$$A_k = K_{k-1,k} f_k A_{k-1} \quad k > 1, \quad (17)$$

$$A_1 = \sum_{s_0^\pm} K_{01} f_1(s_0^+ | \rho(0) | s_0^-). \quad (18)$$

The reduced density matrix of the system can be calculated from ARDT,

$$\rho_S(k\Delta t) = \sum_{s_1^\pm, \dots, s_{k-1}^\pm} A_k. \quad (19)$$

The size of ARDT is exponentially increased with respect to the number of time slices. Even for a two-state system, the affordable number of time slices is less than 20. Fortunately, for a typical condensed phase problem, the physical memory time τ_p is finite, which can be characterized by the bath correlation time. More specifically, the pairwise influence functional $I_{k'k}$ with $k - k' > \tau_p/\Delta t$ will become

1 as $\eta_{k'k}$ approaches 0. In practice, we set a maximal time interval Δk . When $k - k' > \Delta k$, $I_{k'k}$ is discarded. Accordingly, the influence functional is truncated, that is,

$$f_k \approx \tilde{f}_k := \tilde{f}_k(s_{k-\Delta k}^\pm, \dots, s_k^\pm). \quad (20)$$

With this truncation of influence functional, the time slices in ARDT before $k - \Delta k$ will not be used anymore and thus can be integrated. The new iterative equation when $k > \Delta k$ is

$$\tilde{A}_k := \tilde{A}_k(s_{k-\Delta k+1}^\pm, \dots, s_k^\pm), \quad (21)$$

$$\bar{A}_k := \bar{A}_k(s_{k-\Delta k}^\pm, \dots, s_k^\pm), \quad (22)$$

$$\bar{A}_k = K_{k-1,k} \tilde{f}_k \tilde{A}_{k-1}, \quad \tilde{A}_{\Delta k} = A_{\Delta k}, \quad (23)$$

$$\tilde{A}_k = \sum_{s_{k-\Delta k}^\pm} \bar{A}_k, \quad (24)$$

$$\rho_S(k\Delta t) = \sum_{s_{k-\Delta k+1}^\pm, \dots, s_{k-1}^\pm} \tilde{A}_k. \quad (25)$$

Following these iterative equations, Eqs. (23) and (24), ARDT \tilde{A}_k will propagate with a fixed size $d^{\Delta k}$, where d is the size of the system Hilbert space. This method is called iterative QuAPI. It should be noted that the intermediate tensor \bar{A} does not have to be stored in the actual implementation. Here, we keep it to make it easier to compare to the new memory truncation scheme later. The schematic diagram of conventional iQuAPI is shown in Fig. 1(a).

It should be emphasized that only when the preset maximal time interval is longer than the physical memory time ($\Delta k \Delta t > \tau_p$), this memory truncation scheme in original iQuAPI is exact. Otherwise, it is an approximation, called finite memory approximation. Because the physical memory time is not known in advance, in practice, several different Δk should be calculated to check the convergence. It has been reported and will be shown in Sec. III that for problems with a pretty long physical memory time, the results converge very slowly with Δk and sometimes cannot even converge in an affordable amount of computational cost. Therefore, we need a better memory truncation scheme. This is the motivation of this work.

B. Memory truncation scheme based on DMRG

The main idea to improve the conventional truncation scheme is that the influence functional beyond Δk is not fully discarded, but is renormalized, and then, the most important part of it is selected and retained. The renormalization step is inspired by the density matrix renormalization group theory^{44,45} and accomplished by the singular value decomposition (SVD) algorithm.

When the time step $k = \Delta k + 1$ (the first truncation step is a bit different from the following steps), instead of summing $\tilde{A}_{\Delta k+1}$ over s_1^\pm as in conventional iQuAPI [Eq. (24)], $\tilde{A}_{\Delta k+1}$ after unfolding is decomposed by SVD as

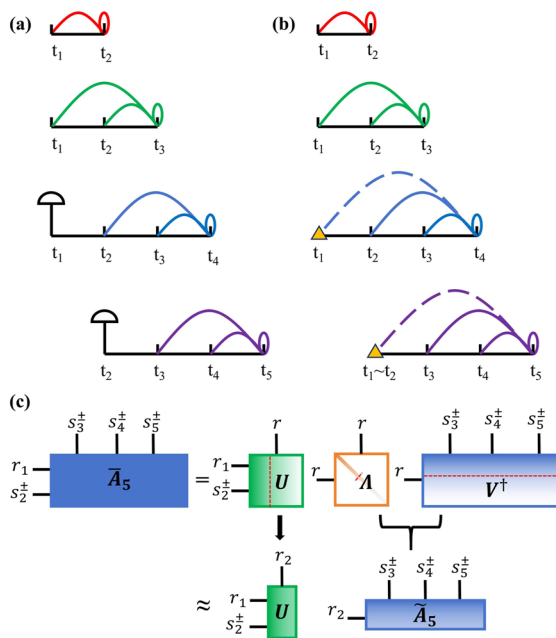


FIG. 1. Schematic diagram of iQuAPI with (a) the conventional memory truncation scheme and (b) the improved memory truncation scheme based on DMRG. $\Delta k = 2$. The lines in different colors represent the pairwise influence functional subterms $I_{k'k}$. A solid/dashed line indicates that the subterm is exact/approximated. The semicircle represents the summation of the time slices beyond the truncation length. The triangle represents the auxiliary time slice that contains partial information of the history. (c) The graphic diagram of the renormalization process when $k = 5$. After SVD, the deeper color in U, Λ, V^\dagger indicates more important components.

$$\tilde{A}_{\Delta k+1} \rightarrow \tilde{A}_{\Delta k+1}(s_1^\pm | s_2^\pm \cdots s_{\Delta k+1}^\pm) = \sum_{r=1}^n U_{s_1^\pm, r} \Lambda_r V_{r, s_2^\pm \cdots s_{\Delta k+1}^\pm}^\dagger \\ \approx \sum_{r_1=1}^{M_1} U_{s_1^\pm, r_1} \Lambda_{r_1} V_{r_1, s_2^\pm \cdots s_{\Delta k+1}^\pm}^\dagger, \quad (26)$$

where U and V are column-wise orthonormal matrices. Λ is a diagonal matrix with real and non-negative diagonal elements ($\Lambda_1 \geq \Lambda_2 \geq \cdots \geq \Lambda_n \geq 0$), called singular values. In the first truncation step, $n = d^2$. Instead of keeping all the n components, we set a cutoff ξ and select only the components with $\Lambda_r / \sqrt{\sum_r \Lambda_r^2} > \xi$, the size of which is M_1 . This selection minimizes the Euclidean distance between the original ARDT and the approximated ARDT. After this selection, the state $|s_1^\pm\rangle$ is renormalized to $|r_1\rangle$ according to $U_{s_1^\pm, r_1}$,

$$|r_1\rangle = \sum_{s_1^\pm} |s_1^\pm\rangle U_{s_1^\pm, r_1}, \quad (27)$$

where $|r_1\rangle$ can be regarded as the basis states of the auxiliary time slice. The renormalized ARDT is defined as

$$\tilde{A}_{\Delta k+1}(r_1, s_2^\pm, \dots, s_{\Delta k+1}^\pm) = \Lambda_{r_1} V_{r_1, s_2^\pm \cdots s_{\Delta k+1}^\pm}^\dagger. \quad (28)$$

In addition, the pairwise influence functional between s_1^\pm and k'' ($k'' > \Delta k + 1$) is renormalized as

$$\tilde{I}_{1k''}(r_1, r'_1, s_{k''}^\pm) = \sum_{s_1^\pm} U_{r_1, s_1^\pm}^\dagger I_{1k''}(s_1^\pm, s_{k''}^\pm) U_{s_1^\pm, r'_1}, \quad (29)$$

where $\tilde{I}_{1k''}(r_1, r'_1, s_{k''}^\pm)$ is the influence functional between the auxiliary time slice and normal time slice k'' , which is a three-legged tensor different from the original one. Correspondingly,

$$\tilde{f}_{k''}(r_1, r'_1, s_2^\pm, \dots, s_{k''}^\pm) = \tilde{I}_{1k''} \prod_{k'=2}^{k''} I_{k'k''}. \quad (30)$$

To calculate the reduced density matrix of the system at this time, it should be noted that the renormalized states $|r_1\rangle$ have a different weight to the original $|s_1^\pm\rangle$. The weight is

$$W_1(r_1) = \sum_{s_1^\pm} U_{s_1^\pm, r_1}, \quad (31)$$

therefore,

$$\rho((\Delta k + 1)\Delta t) = \sum_{r_1, s_2^\pm, \dots, s_{\Delta k}^\pm} W_1(r_1) \tilde{A}_{\Delta k+1}(r_1, s_2^\pm, \dots, s_{\Delta k+1}^\pm). \quad (32)$$

It can be checked that when r_1 is not truncated ($\xi = 0, M_1 = d^2$), $\rho((k+1)\Delta t)$ is exact because only a unitary basis rotation between $|s_1^\pm\rangle$ and $|r_1\rangle$ is performed, which does not alter the results. (See the [supplementary material](#) for the proof.)

The renormalization step will continue iteratively. When $k > \Delta k + 1$,

$$\tilde{A}_k := \tilde{A}_k(r_{k-\Delta k}, s_{k-\Delta k+1}^\pm, \dots, s_k^\pm), \quad (33)$$

$$\tilde{A}_k := \tilde{A}_k(r_{k-\Delta k-1}, s_{k-\Delta k}^\pm, \dots, s_k^\pm), \quad (34)$$

$$\tilde{A}_k = \sum_{r'_{k-\Delta k}} K_{k-1, k} \tilde{f}_k \tilde{A}_{k-1}(r'_{k-\Delta k-1}, s_{k-\Delta k}^\pm, \dots, s_{k-1}^\pm). \quad (35)$$

Similar as Eq. (26),

$$\tilde{A}_k \rightarrow \tilde{A}_k(r_{k-\Delta k-1} s_{k-\Delta k}^\pm | s_{k-\Delta k+1}^\pm \cdots s_k^\pm) \\ \approx \sum_{r_{k-\Delta k}=1}^{M_{k-\Delta k}} U_{r_{k-\Delta k-1} s_{k-\Delta k}^\pm, r_{k-\Delta k}} \Lambda_{r_{k-\Delta k}} V_{r_{k-\Delta k}, s_{k-\Delta k+1}^\pm \cdots s_k^\pm}^\dagger, \quad (36)$$

$$\tilde{A}_k = \Lambda_{r_{k-\Delta k}} V_{r_{k-\Delta k}, s_{k-\Delta k+1}^\pm \cdots s_k^\pm}^\dagger. \quad (37)$$

The state $|r_{k-\Delta k-1} \otimes s_{k-\Delta k}^\pm\rangle$ is renormalized to $|r_{k-\Delta k}\rangle$ according to $U_{r_{k-\Delta k-1} s_{k-\Delta k}^\pm, r_{k-\Delta k}}$,

$$|r_{k-\Delta k}\rangle = \sum_{r_{k-\Delta k-1} s_{k-\Delta k}^\pm} |r_{k-\Delta k-1} s_{k-\Delta k}^\pm\rangle U_{r_{k-\Delta k-1} s_{k-\Delta k}^\pm, r_{k-\Delta k}}. \quad (38)$$

The pairwise influence functional between $r_{k-\Delta k-1}$ and k'' ($k'' > k$), together with the pairwise influence functional between $s_{k-\Delta k}^\pm$ and k'' , is renormalized to

$$\tilde{I}_{k-\Delta k, k''} := \tilde{I}_{k-\Delta k, k''}(r_{k-\Delta k}, r'_{k-\Delta k}, s_{k-\Delta k}^\pm), \quad (39)$$

$$\begin{aligned} \tilde{I}_{k-\Delta k, k''} = & \sum_{r_{k-\Delta k-1}, r'_{k-\Delta k-1}, s_{k-\Delta k}^\pm} U_{r_{k-\Delta k}, r_{k-\Delta k-1}, s_{k-\Delta k}^\pm}^\dagger \\ & \times \tilde{I}_{k-\Delta k-1, k''} I_{k-\Delta k, k''} U_{r'_{k-\Delta k-1}, s_{k-\Delta k}^\pm, r'_{k-\Delta k}}. \end{aligned} \quad (40)$$

Correspondingly,

$$\tilde{f}_{k+1} = \tilde{I}_{k-\Delta k, k+1} \prod_{k'=k-\Delta k+1}^{k+1} I_{k', k+1}. \quad (41)$$

It should be noted that only the pairwise influence functional between $k - \Delta k$ and k'' ($k'' > k$) should be renormalized because the others between $k - \Delta k$ and k'' ($k'' \leq k$) within the memory truncation length have already been considered exactly.

The weight of the renormalized states $|r_{k-\Delta k}\rangle$ is

$$W_{k-\Delta k} := W_{k-\Delta k}(r_{k-\Delta k}), \quad (42)$$

$$W_{k-\Delta k} = \sum_{r_{k-\Delta k-1}, s_{k-\Delta k}^\pm} W_{k-\Delta k-1} U_{r_{k-\Delta k-1}, s_{k-\Delta k}^\pm, r_{k-\Delta k}}. \quad (43)$$

The reduced density matrix of the system is

$$\rho(k\Delta t) = \sum_{r_{k-\Delta k}, s_{k-\Delta k+1}^\pm, \dots, s_{k-1}^\pm} W_{k-\Delta k} \tilde{A}_k. \quad (44)$$

The overall algorithm is shown in Algorithm 1. The arrows in Algorithm 1 indicate that the variables on the left are calculated from the variables on the right, based on the equation that follows. The schematic diagram is shown in Figs. 1(b) and 1(c). Figure 1(c) shows the following key steps in the renormalization process: (i) unfolding ARDT by separating the auxiliary time slice and the leftmost normal time slice from the other time slices; (ii) decomposing ARDT by SVD and retaining only the dominant components to form the new auxiliary time slice and basis states.

Compared to the memory truncation scheme in the original iQuAPI, where the influence functional is sharply truncated when the time interval exceeds a preset $\Delta k\Delta t$, the new truncation scheme introduces an auxiliary time slice. The renormalized pairwise influence functional between the auxiliary time slice and the future time slices retains the most important memory effect beyond the preset maximal time interval, although it is not exact. As a result, we expect that the new memory truncation scheme can improve the results of conventional iQuAPI, especially for problems with long memory. Due to the different features of these two truncation schemes, we refer to the new truncation scheme as the soft truncation scheme (ST) and the conventional truncation scheme as the hard truncation scheme (HT) in the following.

In ST-QuAPI, the basis states of the auxiliary time slice are renormalized recursively and selected adaptively during the time

ALGORITHM 1. iQuAPI algorithm with a memory truncation scheme based on DMRG.

```

1: procedure PREPARE SYSTEM PROPAGATOR ( $\hat{H}_1, \Delta t$ )
2:    $K_{k-1,k} \leftarrow \hat{H}_1, \Delta t$                                  $\triangleright$  Eq. (10)
3:   return  $K_{k-1,k}$ 
4: end procedure

5: procedure PREPARE INFLUENCE FUNCTIONAL ( $\eta_{k'k}$ )
6:   for  $k = 1 \rightarrow N$  do
7:     for  $k' = 1 \rightarrow k$  do
8:        $I_{k'k} \leftarrow \eta_{k'k}$                                  $\triangleright$  Eq. (12)
9:        $f_k \leftarrow I_{k'k}$                                  $\triangleright$  Eq. (15)
10:      end for
11:    end for
12:   return  $I_{k'k}, f_k$ 
13: end procedure

14: procedure EVOLUTION PROCESS ( $I_{k'k}, f_k, K_{k-1,k}$ )
15:    $A_1, \rho(\Delta t) \leftarrow K_{01}, f_1, \rho(0)$                  $\triangleright$  Eq. (18)
16:   for  $k = 2 \rightarrow N$  do
17:     if  $k \leq \Delta k$  then
18:        $A_k \leftarrow A_{k-1}, f_k, K_{k-1,k}$                        $\triangleright$  Eq. (17)
19:        $\rho(k\Delta t) \leftarrow A_k$                                  $\triangleright$  Eq. (19)
20:       if  $k = \Delta k$ ,  $\tilde{A}_{\Delta k}, \tilde{f}_{\Delta k+1} \leftarrow A_{\Delta k}, f_{\Delta k+1}$ 
21:     else
22:        $\tilde{A}_k \leftarrow \tilde{A}_{k-1}, \tilde{f}_k, K_{k-1,k}$            $\triangleright$  Eq. (35)
23:        $U, \Lambda, V^\dagger \leftarrow \text{SVD}[\tilde{A}_k]$              $\triangleright$  Eq. (36)
24:        $\tilde{A}_k \leftarrow \Lambda, V^\dagger$                              $\triangleright$  Eq. (37)
25:        $\tilde{I}_{k-\Delta k, k''} \leftarrow U, \tilde{I}_{k-\Delta k-1, k''}, I_{k-\Delta k, k''}$   $\triangleright$  Eq. (40)
26:        $\tilde{f}_{k+1} \leftarrow \tilde{I}_{k-\Delta k, k+1}, I_{k', k+1}$             $\triangleright$  Eq. (41)
27:        $W_{k-\Delta k} \leftarrow U, W_{k-\Delta k-1}$                    $\triangleright$  Eq. (43)
28:        $\rho(k\Delta t) \leftarrow W_{k-\Delta k}, \tilde{A}_k$                $\triangleright$  Eq. (44)
29:     end if
30:   end for
31:   return  $\rho(k\Delta t)$ 
32: end procedure

```

propagation according to the singular values Λ_r of ARDT and the preset cutoff ξ . Unlike HT-QuAPI in which only the parameter Δk determines the accuracy, in ST-QuAPI, the SVD cutoff ξ also determines the accuracy. When the cutoff ξ is 0, meaning that all the basis states are retained, the approach reverts to the exact QuAPI no matter what Δk is, yielding exact results since any unitary transformation between the basis states does not alter the results. Otherwise, the distribution of the singular values Λ_r with the index of renormalized state r is very important, which characterizes the strength of temporal correlation. When Λ_r decays very fast with r , only a small number of renormalized states need to be retained; in this case, the new truncation scheme is effective. When Λ_r decays very slowly with r , a large number of renormalized states should be retained to ensure a high accuracy. The worst case is that Λ_r is equal for different r , indicating that the temporal correlation between the historical time slices and future time slices at this time point is extremely strong. In this case, all the states must be retained and any truncation scheme is invalid.

We briefly analyze the computational scaling of the ST-QuAPI method. For HT-QuAPI, the computational scaling is $O(d^{2\Delta k})$ from the contraction of $A_{k-1}f_k K_{k-1,k}$. Compared to HT-QuAPI, the contraction in ST-QuAPI scales as $O(M^2 d^{2\Delta k})$ because of the extra auxiliary time slice. In addition, an SVD process is needed to obtain the renormalized basis states in each time step, whose scaling is also $O(M^2 d^{2\Delta k})$. Thus, the overall computational scaling of ST-QuAPI is $O(M^2 d^{2\Delta k})$. In addition to the computational cost, the memory requirement to store the high dimensional tensor in ST-QuAPI is $O(Md^{2\Delta k})$, while that in HT-QuAPI is $O(d^{2\Delta k})$. Although the formal scaling of ST-QuAPI seems larger than that of HT-QuAPI, the size of Δk is much smaller for ST-QuAPI than HT-QuAPI to get converged results.

Before closing this section, we will briefly discuss the relation between our memory truncation scheme and TEMPO. As mentioned in the Introduction section, TEMPO takes advantage of matrix product states (MPS) to approximate ARDT thereby preventing ARDT from growing exponentially with time steps. Similarly, the iterative renormalization step in our memory truncation scheme also essentially constructs an MPS. The main difference lies in that in our approach, the renormalization matrices are fixed beyond the truncation length, while the matrices of MPS in TEMPO are all allowed to be optimized. This difference is similar to that between infinite DMRG and finite DMRG.⁵² Although allowing the matrices to be optimized makes TEMPO more accurate, it is more expensive for long-time dynamics. Therefore, in practical calculations by

TEMPO, the conventional memory truncation scheme is still being used.³³ In this regard, our new memory truncation scheme is compatible with TEMPO to replace the currently used scheme to make it more accurate to capture the memory effect. In other words, we can use TEMPO to approximate the exact part of ARDT in ST-QuAPI to enlarge the parts where the influence functional is treated exactly.

III. RESULTS

In this section, we benchmark the new truncation scheme in the spin-boson model (SBM). SBM is one of the most celebrated models to study quantum dissipative dynamics in the condensed phase.^{1,53} It serves as a testbed to benchmark different quantum dynamics methods. The Hamiltonian of SBM is written as

$$\hat{H} = \varepsilon \hat{\sigma}_z + \Delta \hat{\sigma}_x + \sum_i \frac{1}{2} (\hat{p}_i^2 + \omega_i^2 \hat{x}_i^2) + \hat{\sigma}_z \sum_i c_i \hat{x}_i. \quad (45)$$

We consider four cases with different parameters.

A. SBM with Debye spectral density

The first two cases adopt the Debye spectral density, $J(\omega) = \eta \frac{\omega \omega_c}{\omega + \omega_c}$. $\Delta = 1$ is used as the unit. Case I has a low temperature $\beta = 50$ and fast bath motion $\omega_c = 5$; Case II has a high temperature $\beta = 0.5$ and slow bath motion $\omega_c = 0.25$. The other parameters are

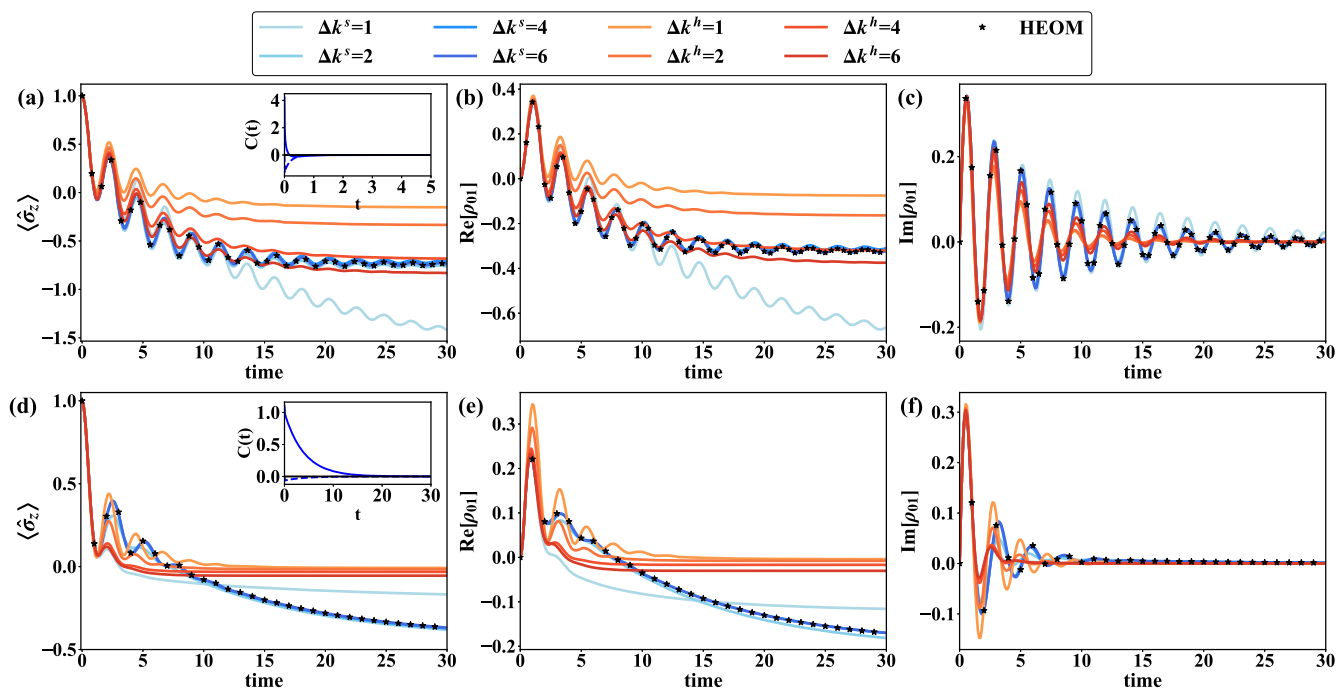


FIG. 2. Reduced density matrix $\rho_S(t)$ of SBM with Debye spectral density. (a)–(c) $\langle \hat{\sigma}_z(t) \rangle$, $\text{Re}[\rho_{01}(t)]$, and $\text{Im}[\rho_{01}(t)]$ of SBM with $\beta = 50$, $\omega_c = 5$ calculated by ST-QuAPI (blue lines) and HT-QuAPI (conventional iQuAPI, red lines) with different truncation lengths $\Delta k = 1, 2, 4, 6$. The black asterisk is the reference calculated by HEOM. The inset is the bath time correlation function (the solid line is the real part, and the dashed line is the imaginary part). Panels (d)–(f) are the same as panels (a)–(c) but with parameter $\beta = 0.5$, $\omega_c = 0.25$.

$\varepsilon = 1$ and $\eta = 0.5$.^{54,55} We simulate the spin dynamics by iQuAPI with the proposed soft memory truncation scheme and the conventional hard truncation scheme. The reference results are calculated with HEOM by QuTiP⁵⁶ with $K = 70, L = 3$ for Case I using Padé expansion and $K = 4, L = 20$ for Case II using Matsubara expansion.

Figures 2(a) and 2(c) show $\langle \hat{\sigma}_z(t) \rangle$ of these two cases with different Δk . The truncation cutoff of ST is $\xi = 10^{-5}$. The time step size is 0.1. The insets are the bath time correlation function of the two cases characterizing the length of memory time,

$$C(t) = \frac{1}{\pi} \int_0^\infty d\omega J(\omega) \left[\coth \frac{\beta\omega}{2} \cos \omega t - i \sin \omega t \right]. \quad (46)$$

Case II with slow bath motion has a relatively long memory time (>10), while Case I with fast bath motion has a short memory time (<1). For the short memory case, ST (blue line) converges much faster than HT (red line) with respect to Δk . When $\Delta k = 6$, ST has achieved an accuracy where the maximal absolute error ε_m is smaller than 0.01 within $t \leq 30$. For comparison, when $\Delta k = 6$, even though the curve of HT is qualitatively correct, ε_m is about 0.1. Even when $\Delta k = 13$, ε_m is ~ 0.03 . For the long memory case, the improvement of ST is much more pronounced. With HT, the convergence of $\langle \hat{\sigma}_z(t) \rangle$ with Δk is very slow. In addition, the asymptotic behavior with t seems totally wrong. On the contrary, the error of ST is greatly reduced even with a very small Δk . With $\Delta k = 6$, ε_m has already been smaller than 0.02. In addition to the diagonal elements of the reduced density matrix, the off-diagonal matrix elements are shown in Figs. 2(b)–2(f). The off-diagonal matrix elements characterize the coherence between the two system states and are believed to be more difficult to calculate accurately than the diagonal elements. In both of these cases, ST can obtain coherence much more accurately than HT with the same Δk . Compared to HT, the improvement in both population and coherence demonstrates that the most important memory effect is indeed captured by the renormalization process in ST as expected. This improvement is essential for problems with long memory time as Case II shown in Figs. 2(d)–2(f).

In addition to Δk , the cutoff ξ in SVD is also important for the accuracy of ST-QuAPI. To evaluate the error brought by SVD cutoffs, we set a series of cutoffs with the same $\Delta k = 6$ for the long memory case, Case II. In Fig. 3(a), we will get more accurate results if we take a smaller cutoff. With $\xi < 10^{-4}$, the maximal absolute error is less than 0.02. In Fig. 3(b), the number of renormalized states of the auxiliary time slice grows rapidly at the beginning (during the time comparable with the bath correlation time), and then, it reaches a certain value that will become larger as the cutoff ξ decreases. The final number of renormalized states is $15 \sim 25$.

To monitor the decay of singular values Λ_r , which indicates the strength of temporal correlation, we show the singular values at several time steps in Fig. 3(c). Overall, with the parameters we considered, the singular values decay quickly with the index of renormalized states. Moreover, although the singular values increase with time suggesting the increase in temporal correlation, they gradually converge to a certain value, meaning that the temporal correlation is bounded with time. This is consistent with what is observed in the number of kept renormalized states with a fixed cutoff shown in Fig. 3(b). The two observations in Fig. 3(c) show that the singular values decay fast and the temporal correlation is

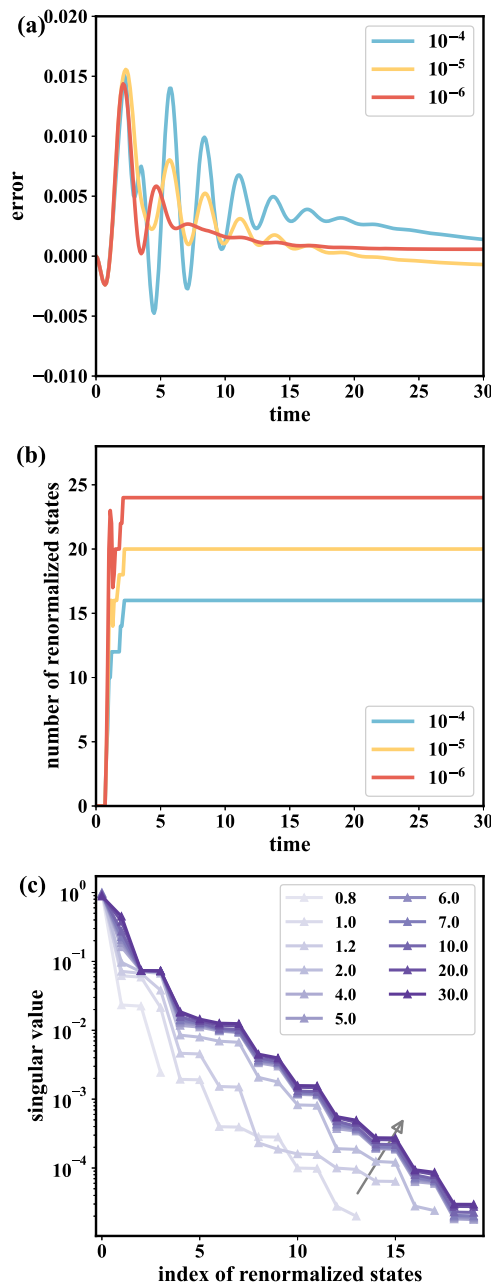


FIG. 3. (a) Error of $\langle \hat{\sigma}_z(t) \rangle$ and (b) the number of renormalized states of the auxiliary time slice with SVD cutoff $\xi = 10^{-4}, 10^{-5}, 10^{-6}$ for Case II. (c) The distribution of singular values Λ_r after normalization at different times from $t = 0.8$ to $t = 30$ with $\xi = 10^{-5}$.

bounded, ensuring the effectiveness of the new truncation scheme based on DMRG. The data for Case I are similar to that for Case II (see the supplementary material Fig. S1). However, whether the observation is general for other more challenging parameter regimes needs further investigation.

B. SBM with Ohmic spectral density

The next two cases we select are what have been studied in detail by Makri in Ref. 43 with the newly developed small matrix path integral with extended memory approach (x-SMatPI). It has been shown that the results calculated by the conventional iQuAPI approach ($\Delta k = 18$) are far from the converged results. We use ST-QuAPI to simulate the dynamics of the two cases and compare the results to that of x-SMatPI. Ohmic spectral density is adopted in these two case, $J(\omega) = \frac{1}{2}\pi\alpha\omega e^{-\omega/\omega_c}$. The parameters are $\varepsilon = 5$, $\Delta = -1$, $\omega_c = 2$, $\alpha = 4$, and $\beta = 0.1$ in Case III and $\varepsilon = 0$, $\Delta = -1$, $\omega_c = 1$, $\alpha = 2$, and $\beta = 1$ in Case IV. The initial bath state is in equilibrium with the up-spin state, which is realized by shifting the coordinate of the system in our simulation.⁵⁷ The time step size and cutoff is $\Delta t = 0.03$ and $\xi = 10^{-6}$ for Case III and $\Delta t = 0.125$ and $\xi = 10^{-6}$ for Case IV, respectively.

Figure 4(a) shows the results for Case III. The population $\rho_{00}(t)$ of ST-QuAPI with $\Delta k = 3$ has already converged within $t < 35$. The black and violet dashed curve is calculated by x-SMatPI with $r = 18$, $\Delta k = 100$ and $r = 18$, $\Delta k = 50$. In SMatPI, r is called the entanglement length, the detailed definition of which can be found in the original paper.⁴³ The larger the value of r , the more accurate is the result. The time step size used in x-SMatPI is $\Delta t = 0.0625$ different from ST-QuAPI. The maximum discrepancy between the result of ST-QuAPI and the most accurate result of x-SMatPI ($r = 18$, $\Delta k = 100$) is less than 0.01. The number of renormalized states of ST-QuAPI is 4, 12, 17, and 21 with $\Delta k = 1, 2, 3, 4$, respectively. Case IV is more demanding than Case III. Figures 4(b) and 4(c) show $\rho_{00}(t)$ and $\text{Im}\rho_{01}(t)$ for Case IV. The discrepancy between ST-QuAPI with $\Delta k = 7$ and x-SMatPI with $r = 18$, $\Delta k = 100$, $\Delta t = 0.25$ is also smaller than 0.01. The number of renormalized states of ST-QuAPI is 12, 28, 36, 43, 52, and 54 with Δk from 2 to 7, respectively. The comparison between these two approaches not only demonstrates the correctness of the results but also reveals the effectiveness of ST-QuAPI in capturing the long memory effect by influence functional renormalization.

IV. CONCLUSION AND OUTLOOK

In this work, we propose a new memory truncation scheme for iterative QuAPI to simulate the quantum dynamics of system–bath coupled problems. The conventional memory truncation scheme used in iterative QuAPI discards all the influence functional beyond a preset time interval, which is not effective for problems with long memory time. Instead, our memory truncation scheme selects and retains the most important parts of the originally discarded influence functional to improve the accuracy. The criterion for selection is to minimize the difference between the augmented reduced density tensor before and after truncation, realized by the density matrix renormalization group algorithm. As a result, an auxiliary time slice that contains partial information of the history is constructed adaptively and iteratively and so is the influence functional between the effective time slice and future time slices. Therefore, the new memory truncation scheme is more effective than the conventional one, especially for problems with long memory time. This is the main contribution of this work.

We have demonstrated the effectiveness of the improved memory truncation scheme by simulating the quantum dynamics of the spin–boson model. Four different parameter sets are adopted, including Debye spectral density and Ohmic spectral density. In all four cases, our scheme converges much more quickly with the truncation length than the conventional memory truncation scheme. By examining the singular values of ARDT over time, whose distribution characterizes the temporal correlation of the system, we found that in the studied cases, the singular values decay quickly with the indices of renormalized states and the total temporal correlation over time is bounded. This observation indicates the effectiveness of selecting basis states via the DMRG algorithm.

Essentially, our new memory truncation scheme is an improved version of iQuAPI. Any other method that can be combined with iQuAPI can also be combined with our method to handle problems with a much longer memory. For instance, by applying it to calculate the dynamical maps within the memory length, we

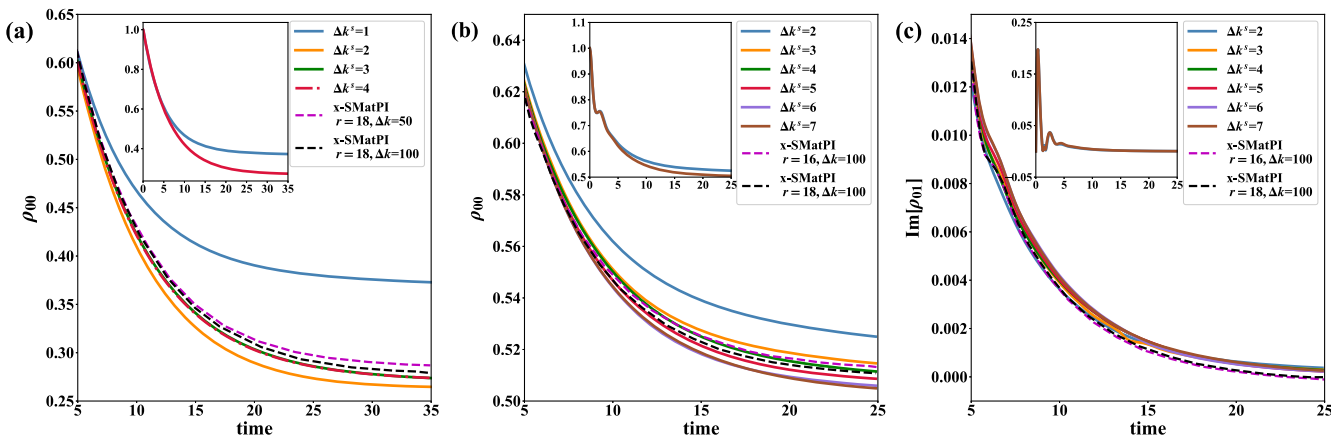


FIG. 4. (a) Population $\rho_{00}(t)$ for SBM Case III and (b) $\rho_{00}(t)$ and (c) $\text{Im}\rho_{01}$ for SBM Case IV calculated by ST-QuAPI with SVD cutoff $\xi = 10^{-6}$ and with different Δk . The dashed lines are the result calculated by x-SMatPI in Ref. 43. The detailed parameters of SBM and other setups are given in the text.

can propagate the reduced density matrix to arbitrarily long times with the transfer tensor method.⁵⁸ Our method is also compatible with the recently developed time-evolving matrix product operator approach.³³ TEMPO uses a matrix product state to approximate the exponentially large augmented reduced density tensor, thereby greatly reducing the computational cost, especially suitable for problems with multiple system states and long memory time. The same truncation scheme as iQuAPI has been adopted to simulate long-time dynamics. We expect that with our truncation scheme, the accuracy of TEMPO will further increase. Related studies are currently being carried out in our group.

SUPPLEMENTARY MATERIAL

See the [supplementary material](#) for the proof of exactness of ST-QuAPI when $\xi = 0$ and the change of the number of renormalized states and singular value distribution with time of SBM Case I as shown in [Fig. 3](#).

ACKNOWLEDGMENTS

The authors thank Professor Jiushu Shao for the insightful discussion. This work was supported by the Innovation Program for Quantum Science and Technology (Grant No. 2023ZD0300200), the National Natural Science Foundation of China (Grant No. 22273005), NSAF (Grant No. U2330201), and the Fundamental Research Funds for the Central Universities.

AUTHOR DECLARATIONS

Conflict of Interest

The authors have no conflicts to disclose.

Author Contributions

Limin Liu: Investigation (equal); Writing – original draft (equal); Writing – review & editing (equal). **Jiajun Ren:** Conceptualization (lead); Investigation (equal); Supervision (equal); Writing – original draft (equal); Writing – review & editing (equal). **Weihai Fang:** Supervision (equal).

DATA AVAILABILITY

The data that support the findings of this study are available from the corresponding author upon reasonable request.

REFERENCES

- ¹A. Nitzan, *Chemical Dynamics in Condensed Phases: Relaxation, Transfer and Reactions in Condensed Molecular Systems* (Oxford University Press, 2006).
- ²A. Ishizaki and G. R. Fleming, “Theoretical examination of quantum coherence in a photosynthetic system at physiological temperature,” *Proc. Natl. Acad. Sci. U. S. A.* **106**, 17255–17260 (2009).
- ³Y. Yan, Y. Liu, T. Xing, and Q. Shi, “Theoretical study of excitation energy transfer and nonlinear spectroscopy of photosynthetic light-harvesting complexes using the nonperturbative reduced dynamics method,” *Wiley Interdiscip. Rev.: Comput. Mol. Sci.* **11**, e1498 (2021).
- ⁴Y.-C. Wang, Y. Ke, and Y. Zhao, “The hierarchical and perturbative forms of stochastic Schrödinger equations and their applications to carrier dynamics in organic materials,” *Wiley Interdiscip. Rev.: Comput. Mol. Sci.* **9**, e1375 (2019).
- ⁵W. Li, J. Ren, and Z. Shuai, “A general charge transport picture for organic semiconductors with nonlocal electron-phonon couplings,” *Nat. Commun.* **12**, 4260 (2021).
- ⁶H. Wang, I. Pshenichnyuk, R. Härtle, and M. Thoss, “Numerically exact, time-dependent treatment of vibrationally coupled electron transport in single-molecule junctions,” *J. Chem. Phys.* **135**, 244506 (2011).
- ⁷J. Jin, X. Zheng, and Y. Yan, “Exact dynamics of dissipative electronic systems and quantum transport: Hierarchical equations of motion approach,” *J. Chem. Phys.* **128**, 234703 (2008).
- ⁸H. Wang and M. Thoss, “Multilayer formulation of the multiconfiguration time-dependent hartree theory,” *J. Chem. Phys.* **119**, 1289–1299 (2003).
- ⁹H. Wang and M. Thoss, “Numerically exact quantum dynamics for indistinguishable particles: The multilayer multiconfiguration time-dependent hartree theory in second quantization representation,” *J. Chem. Phys.* **131**, 024114 (2009).
- ¹⁰H. Ma, Z. Luo, and Y. Yao, “The time-dependent density matrix renormalisation group method,” *Mol. Phys.* **116**, 854–868 (2018).
- ¹¹J. Ren, W. Li, T. Jiang, Y. Wang, and Z. Shuai, “Time-dependent density matrix renormalization group method for quantum dynamics in complex systems,” *Wiley Interdiscip. Rev.: Comput. Mol. Sci.* **12**, e1614 (2022).
- ¹²H.-P. Breuer, E.-M. Laine, J. Piilo, and B. Vacchini, “Colloquium: Non-Markovian dynamics in open quantum systems,” *Rev. Mod. Phys.* **88**, 021002 (2016).
- ¹³M. Sonner, A. Lerose, and D. A. Abanin, “Influence functional of many-body systems: Temporal entanglement and matrix-product state representation,” *Ann. Phys.* **435**, 168677 (2021).
- ¹⁴Y. Tanimura, “Numerically ‘exact’ approach to open quantum dynamics: The hierarchical equations of motion (HEOM),” *J. Chem. Phys.* **153**, 020901 (2020).
- ¹⁵Y.-a. Yan, F. Yang, Y. Liu, and J. Shao, “Hierarchical approach based on stochastic decoupling to dissipative systems,” *Chem. Phys. Lett.* **395**, 216–221 (2004).
- ¹⁶Q. Shi, L. Chen, G. Nan, R.-X. Xu, and Y. Yan, “Efficient hierarchical Liouville space propagator to quantum dissipative dynamics,” *J. Chem. Phys.* **130**, 084105 (2009).
- ¹⁷N. Makri, “Improved Feynman propagators on a grid and non-adiabatic corrections within the path integral framework,” *Chem. Phys. Lett.* **193**, 435–445 (1992).
- ¹⁸N. Makri and D. E. Makarov, “Tensor propagator for iterative quantum time evolution of reduced density matrices. I. Theory,” *J. Chem. Phys.* **102**, 4600–4610 (1995).
- ¹⁹N. Makri and D. E. Makarov, “Tensor propagator for iterative quantum time evolution of reduced density matrices. II. Numerical methodology,” *J. Chem. Phys.* **102**, 4611–4618 (1995).
- ²⁰W. T. Strunz, L. Diósi, and N. Gisin, “Open system dynamics with non-Markovian quantum trajectories,” *Phys. Rev. Lett.* **82**, 1801 (1999).
- ²¹Y.-A. Yan and J. Shao, “Stochastic description of quantum brownian dynamics,” *Front. Phys.* **11**, 110309–110324 (2016).
- ²²E. Mulvihill and E. Geva, “A road map to various pathways for calculating the memory kernel of the generalized quantum master equation,” *J. Phys. Chem. B* **125**, 9834–9852 (2021).
- ²³Q. Shi and E. Geva, “A new approach to calculating the memory kernel of the generalized quantum master equation for an arbitrary system–bath coupling,” *J. Chem. Phys.* **119**, 12063–12076 (2003).
- ²⁴R. P. Feynman and F. Vernon, Jr., “The theory of a general quantum system interacting with a linear dissipative system,” *Ann. Phys.* **281**, 547–607 (2000).
- ²⁵S. Kundu and N. Makri, “Real-time path integral simulation of exciton-vibration dynamics in light-harvesting bacteriochlorophyll aggregates,” *J. Phys. Chem. Lett.* **11**, 8783–8789 (2020).

- ²⁶S. Kundu, R. Dani, and N. Makri, "Tight inner ring architecture and quantum motion of nuclei enable efficient energy transfer in bacterial light harvesting," *Sci. Adv.* **8**, eadd0023 (2022).
- ²⁷S. Kundu and N. Makri, "PATHSUM: A C++ and Fortran suite of fully quantum mechanical real-time path integral methods for (multi-)system + bath dynamics," *J. Chem. Phys.* **158**, 224801 (2023).
- ²⁸A. Strathearn, B. W. Lovett, and P. Kirton, "Efficient real-time path integrals for non-Markovian spin-boson models," *New J. Phys.* **19**, 093009 (2017).
- ²⁹E. Sim, "Quantum dynamics for a system coupled to slow baths: On-the-fly filtered propagator method," *J. Chem. Phys.* **115**, 4450–4456 (2001).
- ³⁰N. Makri, "Iterative blip-summed path integral for quantum dynamics in strongly dissipative environments," *J. Chem. Phys.* **146**, 134101 (2017).
- ³¹M. Richter and B. P. Fingerhut, "Coarse-grained representation of the quasi adiabatic propagator path integral for the treatment of non-Markovian long-time bath memory," *J. Chem. Phys.* **146**, 214101 (2017).
- ³²N. Makri, "Kink sum for long-memory small matrix path integral dynamics," *J. Phys. Chem. B* **128**, 2469–2480 (2024).
- ³³A. Strathearn, P. Kirton, D. Kilda, J. Keeling, and B. W. Lovett, "Efficient non-Markovian quantum dynamics using time-evolving matrix product operators," *Nat. Commun.* **9**, 3322 (2018).
- ³⁴M. R. Jorgensen and F. A. Pollock, "Exploiting the causal tensor network structure of quantum processes to efficiently simulate non-Markovian path integrals," *Phys. Rev. Lett.* **123**, 240602 (2019).
- ³⁵E. Ye and G. K.-L. Chan, "Constructing tensor network influence functionals for general quantum dynamics," *J. Chem. Phys.* **155**, 044104 (2021).
- ³⁶A. Bose and P. L. Walters, "A multisite decomposition of the tensor network path integrals," *J. Chem. Phys.* **156**, 024101 (2022).
- ³⁷N. Ng, G. Park, A. J. Millis, G. K.-L. Chan, and D. R. Reichman, "Real-time evolution of Anderson impurity models via tensor network influence functionals," *Phys. Rev. B* **107**, 125103 (2023).
- ³⁸A. Bose, "Quantum correlation functions through tensor network path integral," *J. Chem. Phys.* **159**, 214110 (2023).
- ³⁹V. Link, H.-H. Tu, and W. T. Strunz, "Open quantum system dynamics from infinite tensor network contraction," *Phys. Rev. Lett.* **132**, 200403 (2024).
- ⁴⁰R. Chen, X. Xu, and C. Guo, "Grassmann time-evolving matrix product operators for quantum impurity models," *Phys. Rev. B* **109**, 045140 (2024).
- ⁴¹N. Makri, "Small matrix disentanglement of the path integral: Overcoming the exponential tensor scaling with memory length," *J. Chem. Phys.* **152**, 041104 (2020).
- ⁴²N. Makri, "Small matrix path integral for system-bath dynamics," *J. Chem. Theory Comput.* **16**, 4038–4049 (2020).
- ⁴³N. Makri, "Small matrix path integral with extended memory," *J. Chem. Theory Comput.* **17**, 1–6 (2021).
- ⁴⁴S. R. White, "Density matrix formulation for quantum renormalization groups," *Phys. Rev. Lett.* **69**, 2863 (1992).
- ⁴⁵S. R. White, "Density-matrix algorithms for quantum renormalization groups," *Phys. Rev. B* **48**, 10345 (1993).
- ⁴⁶N. Makri, "Quantum dissipative dynamics: A numerically exact methodology," *J. Phys. Chem. A* **102**, 4414–4427 (1998).
- ⁴⁷T. Palm and P. Nalbach, "Quasi-adiabatic path integral approach for quantum systems under the influence of multiple non-commuting fluctuations," *J. Chem. Phys.* **149**, 214103 (2018).
- ⁴⁸N. Acharyya, R. Ovcharenko, and B. P. Fingerhut, "On the role of non-diagonal system–environment interactions in bridge-mediated electron transfer," *J. Chem. Phys.* **153**, 185101 (2020).
- ⁴⁹M. Richter and S. Hughes, "Enhanced TEMPO algorithm for quantum path integrals with off-diagonal system-bath coupling: Applications to photonic quantum networks," *Phys. Rev. Lett.* **128**, 167403 (2022).
- ⁵⁰J. Shao and N. Makri, "Iterative path integral calculation of quantum correlation functions for dissipative systems," *Chem. Phys.* **268**, 1–10 (2001).
- ⁵¹J. Shao and N. Makri, "Iterative path integral formulation of equilibrium correlation functions for quantum dissipative systems," *J. Chem. Phys.* **116**, 507–514 (2002).
- ⁵²U. Schollwöck, "The density-matrix renormalization group in the age of matrix product states," *Ann. Phys.* **326**, 96–192 (2011).
- ⁵³A. J. Leggett, S. Chakravarty, A. T. Dorsey, M. P. Fisher, A. Garg, and W. Zwerger, "Dynamics of the dissipative two-state system," *Rev. Mod. Phys.* **59**, 1 (1987).
- ⁵⁴K. Song, L. Song, and Q. Shi, "An alternative realization of the exact non-Markovian stochastic Schrödinger equation," *J. Chem. Phys.* **144**, 224105 (2016).
- ⁵⁵X. Gao, J. Ren, A. Eisfeld, and Z. Shuai, "Non-Markovian stochastic Schrödinger equation: Matrix-product-state approach to the hierarchy of pure states," *Phys. Rev. A* **105**, L030202 (2022).
- ⁵⁶J. Johansson, P. Nation, and F. Nori, "QuTiP 2: A python framework for the dynamics of open quantum systems," *Comput. Phys. Commun.* **184**, 1234–1240 (2013).
- ⁵⁷P. L. Walters, T. Banerjee, and N. Makri, "On iterative path integral calculations for a system interacting with a shifted dissipative bath," *J. Chem. Phys.* **143**, 074112 (2015).
- ⁵⁸J. Cerrillo and J. Cao, "Non-Markovian dynamical maps: Numerical processing of open quantum trajectories," *Phys. Rev. Lett.* **112**, 110401 (2014).